Author Manuscript

Author Manuscript

Author Manuscript

Author Manuscript

HHS Public Access

Author manuscript

Circ Res. Author manuscript; available in PMC 2018 November 10.

Published in final edited form as:

Circ Res. 2017 November 10; 121(11): 1263–1278. doi:10.1161/CIRCRESAHA.117.311174.

Cortical Bone Stem Cell Therapy Preserves Cardiac Structure and Function After Myocardial Infarction

Thomas E. Sharp III[1], **Giana J. Schena**[1], **Alexander R. Hobby**[1], **Timothy Starosta**[1,6], **Remus M. Berretta**[1], **Markus Wallner**[1], **Giulia Borghetti**[1], **Polina Gross**[1], **Daohai Yu**[2], **Jaslyn Johnson**[1], **Eric Feldsott**[1], **Danielle M. Trappanese**[1], **Amir Toib**[1,3], **Joseph E. Rabinowitz**[4], **Jon C. George**[1,6], **Hajime Kubo**[1], **Sadia Mohsin**[1], and **Steven R. Houser**[1]

[1]Department of Physiology, Cardiovascular Research Center, Temple University Lewis Katz School of Medicine, Philadelphia, PA. 19140

[2]Department of Clinical Sciences, Temple Clinical Research Institute, Temple University Lewis Katz School of Medicine, Philadelphia, PA. 19140

[3]Section of Pediatric Cardiology, St. Christopher's Hospital for Children and the Department of Pediatrics, Drexel University College of Medicine, Philadelphia, PA. 19129

[4]Department of Pharmacology, Center for Translational Medicine, Temple University Lewis Katz School of Medicine, Philadelphia, PA. 19140

[5]Department of Cardiology, Temple University Hospital, Philadelphia, PA. 19140

Abstract

Rationale—Cortical bone stem cells (CBSCs) have been shown to reduce ventricular remodeling and improve cardiac function in a murine myocardial infarction (MI) model. These effects were superior to other stem cell types that have been used in recent early stage clinical trials. However, CBSC efficacy has not been tested in a preclinical large animal model using approaches that could be applied to patients.

Objective—To determine if post–MI transendocardial injection of allogeneic CBSCs reduces pathological structural and functional remodeling and prevents the development of heart failure in a swine MI model.

Methods and Results—Female Göttingen swine underwent left anterior descending coronary artery occlusion, followed by reperfusion (ischemia–reperfusion MI). Animals received, in a randomized, blinded manner, 1:1 ratio, CBSCs (n = 9) (2×10^7 cells total) or placebo (vehicle; VEH, n = 9) through NOGA® guided transendocardial injections. 5–ethynyl–2'deoxyuridine (EdU), a thymidine analog, containing minipumps were inserted at the time of MI induction. At 72hrs (n=8) initial injury and cell retention were assessed. At 3 Months post–MI, cardiac structure

Address correspondence to: Dr. Steven R. Houser, Temple University, Lewis Katz School of Medicine, 3500 N. Broad Street, Medical Education Research Building 10th Floor, Philadelphia, PA. 19140, Tel: 215-707-4045, Fax: 215-707-5737, srhouser@temple.edu.

[6]Currently at the Department Cardiology, Johns Hopkins University School of Medicine, Baltimore, MD. 21205

DISCLOSURES

T.E.S. (None), G.S (None), A.R.H (None), T.S. (None), R.M.B (None), M.W. (None), G.B. (None), P.G. (None), D.Y. (None), J.J. (None), E.F. (None), D.M.T. (None), A.T. (None), J.E.R. (None), J.C.G. (None), H.K. (None), S.M. (None), and S.R.H. (None)

Author Manuscript Author Manuscript Author Manuscript Author Manuscript

and function was evaluated by serial echocardiography, and terminal invasive hemodynamics. CBSCs were present in the MI border zone and proliferating at 72hrs post–MI but had no effect on initial cardiac injury or structure. At 3 months, CBSC–treated hearts had significantly reduced scar size, smaller myocytes and increased myocyte nuclear density. Noninvasive echocardiographic measurements showed that left ventricular (LV) volumes and ejection fraction were significantly more preserved in CBSC–treated hearts and invasive hemodynamic measurements documented improved cardiac structure and functional reserve. The number of EdU^+ cardiac myocytes was increased in CBSC– vs. VEH– treated animals.

Conclusions—CBSC administration into the MI border zone reduces pathological cardiac structural and functional remodeling and improves LV functional reserve. These effects reduce those processes that can lead to heart failure with reduced ejection fraction (HFrEF).

Keywords

Basic translational research; acute myocardial infarction; stem cell therapy; left ventricular remodeling; invasive hemodynamics; animal model cardiovascular disease; cell transplantation

INTRODUCTION

Ischemic heart disease (IHD) is the greatest single cause of mortality worldwide, accounting for ~7 million deaths annually[1]. IHD is caused by coronary artery disease (CAD) that frequently results in myocardial infarction (MI). MI causes the death of myocardial tissue, even when blood flow is restored (ischemia followed by reperfusion [I/R]), resulting in a reduction in the number of cardiac myocytes. While mortality, following MI, has improved dramatically in the era of prompt reperfusion therapy[2], the infarcted tissue is largely replaced by scar and the resultant cardiac structural and functional remodeling causes progressive declines in cardiac pump function[3] that can lead to heart failure (HF). Novel therapeutic strategies that reduce pathological post–MI structural and functional remodeling, and thereby prevent HF development are needed.

A variety of cell therapies have been studied with the goal to enhance vascularization of the ischemic heart[4–6] and/or to replace lost cardiac myocytes[7–10]. Most of these studies have shown small improvements in cardiac structure and function and a few have shown evidence for myogenesis[11, 12]. However, effects observed to date have been modest and there is a need for novel cell therapies with a well-documented ability to reduce adverse post–MI remodeling. In addition, issues including cell safety, dosing, time and route of delivery, in our view, still have not been adequately defined.

Studies in rodent models, utilizing different cell types and multiple delivery techniques, have overwhelmingly suggested that cell therapy can attenuate post–MI remodeling[13–15]. However, studies in preclinical large animal models and early phase I and II clinical trials[11, 16–23] have generally shown more modest effects. Importantly, early stage clinical trials have demonstrated the safety of cell therapy in post–MI patients[21, 23–25] or in patients with established cardiac disease[22, 26, 27].

Author Manuscript Author Manuscript Author Manuscript Author Manuscript

We have identified a novel stem cell population, isolated from cortical bone, and have shown that these cells have cardio-protective features, both in vitro[28] and in vivo[29]. Cortical bone stem cells (CBSCs) were found to be distinct from cardiac–derived stem cells (CDCs) and mesenchymal stem cells (MSCs), and they possess characteristics that account for their in vivo cardio–protective features[28]. CBSCs improved post–MI survival, reduced scar size, reduced ventricular dilation and improved cardiac function when transplanted into the MI border zone of a mouse model[29], and their effects were superior to those of CDCs, both in vitro and in vivo[28, 29].

The present study was designed to test the hypothesis that injection of CBSCs, into the border zone, in a large animal model (swine) of an I/R induced MI reduces post–MI structural and functional remodeling and prevents the development of heart failure. The study examined if CBSCs reduced initial cardiac injury (cardioprotection), survived in the MI border zone after transendocardial delivery, and if they reduced post–MI structural and functional remodeling to improve cardiac pump function. These studies used approaches that could be implemented in patients who have suffered an MI and have undergone reperfusion therapy.

METHODS

A full methods section is available in the Online Supplemental. Figure 1 is a timeline of the experiments performed in the study.

RESULTS

IR/MI survival and arrhythmogenic events

Twenty-three animals underwent IR/MI ([72hr cohort n=11] & [3Mon cohort n=12]). Two animals in each group could not be resuscitated due to pulseless electrical activity (PEA) during ischemia. The IR/MI survival rate is 78.3% (Figure 2A). One animal (72hr, VEH–treated cohort) died within 2hrs post-op due to a lethal arrhythmia. All animals who survived longer than 2hrs post-MI survived the entirety of the study (n=18, total). There was no significant difference in body weight at baseline or during follow up (Online Table I & II). Circulating cardiac troponin I (cTnI; upon reperfusion) (Figure 2B) was measured to confirm MI induction and define initial injury. All animals were in sinus rhythm prior to balloon occlusion (Online Figure I A), and showed characteristic ECG changes (ST–segment alterations) after ischemia induction (Online Figure I B & C). Most animals fibrillated (61%) during the MI and were successfully defibrillated (see methods). There were no ventricular arrhythmias observed during the NOGA mapping and injection procedure. No antiarrhythmic agents were required after animals returned to sinus rhythm upon reperfusion (Online Figure I C).

Acute study (72hrs)

Initial injury, apoptosis, safety and efficacy of delivery, and cell retention— Circulating cTnI was elevated at 2hrs post–MI in all animals (Figure 2B), confirming MI induced myocardial necrosis. No differences in 2hr circulating cTnI levels between treatment groups was observed in either short (3 days) or long term (3 Mo) cohorts, showing

Author Manuscript Author Manuscript Author Manuscript Author Manuscript

that the initial IR injury was similar in VEH– and CBSC–treated animals (Figure 2C). Transthoracic ECHO was performed to assess structural and functional changes at 72hrs post IR/MI ± CBSCs. There were no differences in volumetric ECHO–derived parameters and cardiac structural dimensions between treatment groups (Figure 2D–F & Online Figure II). However, when assessing ECHO speckle–tracking strain (Online Figure III), we observed a significant preservation of the longitudinal strain in CBSC– vs. VEH–treated animals (14.52 ± 0.8% [CBSC] vs. 8.7 ± 1.13% [VEH], $p \leq 0.005$) and a preservation in radial strain as compared to baseline (Online Figure III H & I).

Cross–sections of cardiac tissue from explanted hearts were treated with triphenyltetrazolium chloride (TTC), to differentiate metabolically active from necrotic tissue (Figure 2G & H). There were no differences in TTC negative tissue at 72hrs post–MI ± CBSCs (28.1 ± 6.13% [VEH] vs. 27.1 ± 3.73% [CBSC], Figure 2I, $p = ns$). These results clearly show that the extent of myocardial damage caused by I/R in VEH– and CBSC–treated animals was not different. These results also show that CBSC treatment used in these experiments after IR/MI did not cause acute cardio–protection, to reduce the initial infarct size. TUNEL staining and quantification showed a significant reduction in the number of apoptotic non-myocytes per mm^2 in the CBSC–treated vs. VEH–treated animals (Figure 2J). However, there was no significant difference in the number of apoptotic myocytes per mm^2 between groups at 72hrs post–MI (Figure 2K).

A NOGA® mapping system was used to assess electrical conductance within the heart and determine the interface (border zone) between viable and non–viable tissue. The system was also used to guide catheter–based transendocardial injections[30] (Online Figure IV C). Injection sites were observed in explanted hearts with gross visualization of fluorescent microspheres within the myocardium in all eighteen animals in the 72hr and 3Mon cohorts (Online Figure IV D). Between 50–60% of the injection sites were found at the epi– or endo–cardial surfaces in 72hrs and 3Mon post–MI studies (Online Table I & II). Transendocardial injections induced occasional pre–ventricular contractions (PVC), but no sustained or lethal ventricular arrhythmias were observed during delivery or during the follow up ± CBSCs. The viability of the CBSCs after passing through the MYOSTAR® injection catheter was confirmed (Online Figure IV).

Tissue from validated injection sites was processed for either molecular or histological analysis. A dual CBSC labeling strategy (GFP and sex–mismatch) was used to identify the CBSCs (Figure 3) and both approaches have been used previously[31–33]. Injection sites from all (8) 72hr post–MI animals were immunostained for GFP, EdU, α–sarcomeric actin and DAPI. GFP^+ CBSCs were identified in all animals at 72hrs post–MI (n=4) (Figure 3A – E). Interestingly, the GFP^+ CBSCs were EdU^+, showing that the cells were alive and proliferative (Figure 3–1, –2, & –3). PCR analysis of tissue from injection sites confirmed the presence of the Y– chromosome in CBSC–treated animals (Figure 3F). These studies show that CBSCs injected into the MI border zone survive and proliferate within the injured tissue, but do not prevent the necrotic injury that is characteristic of IR/MI[30].

Author Manuscript Author Manuscript Author Manuscript Author Manuscript

CBSC treatment increases cell proliferation

EdU was infused into VEH– and CBSC– treated animals (n=4, each) for the first 3 days after MI to identify cells with newly formed DNA (Figure 4). We imaged and quantified the number of EdU^+ cells at 72hrs post–MI ± CBSCs. Confocal images from the IZ, BDZ, RZ and sBDZ of all animals were examined (Figure 4A1–A4 [VEH] & B1–B4[CBSC]) and EdU^+ cells were identified and quantified using Naquantus[34], a novel semi–automated quantification software. We calculated the total number of nuclei ($DAPI^+$ [all cells]), $EdU^{+/}DAPI^+$ cells (total EdU^+ cells), $Actin^+/DAPI^+$ (total myocytes) and $EdU^+/Actin^+/DAPI^+$ cells (EdU^+ myocytes) (Figure 4 & Online Figure V A – D) in each tissue section. A large number of EdU^+ cells were observed 3 days after MI + CBSCs, and the GFP^+ CBSCs were EdU^+. The majority of these EdU^+ cells were non–myocytes (Figure 4 [arrowheads]). EdU^+ non-myocytes were predominately made up of Von Willebrand $Factor^+$ (VWF) cells, $CD45^+$ cells and smooth muscle $actin^+$ (SMA) cells (Online Figure VI). There was a significant 2–fold increase in the percentage of EdU^+ nuclei (Figure 4A & B [arrowheads]) in CBSC– vs. VEH– treated heart in the BDZ (Figure 4C2), with nonsignificant increases in all other regions (Figure 4C1, C3 & C4). A few EdU^+ cardiac myocytes were identified in every heart (Figure 4A4 and 4B2 [arrows]). None of these were GFP^+, so they were not derived from injected CBSCs. There was no significant difference in the percentage of EdU^+ myocytes in CBSC– vs. VEH–treated hearts in the IZ, BDZ and sBDZ (Figure 4D1–D4). Most EdU^+ myocytes were found at or near the border of the infarcted regions.

Long-term study (3 months)

Characterization of calcification, sarcoidosis, foreign bodies and allograft rejection post-MI ± CBSCs—The International Society for Heart and Lung Transplantation (ISHLT) provides guidelines for characterizing the immune response due to an allograft and the potential for rejection[35]. H&E stained sections were analyzed for the severity of the immune cell infiltrate and the degree to which it encroached on parent myocardium (Online Table III). We used tissue sections from regions of the injection site, as well as, non-injection site regions. The VEH – treated animals had a greater incidence of calcification vs. CBSC–treated animals (Online Table III & Online Figure VII). No sarcoidosis was observed in any section. Non-cellular foreign bodies were found within the myocardium of both treatment arms consisting of fluorescent microspheres that were injected during the time of therapy delivery (Online Table III & Online Figure VII). Less immune cell infiltrate was observed at 3Mons post-MI in animals who received CBSC therapy as compared to VEH–treated animals (Online Table III).

Preservation of LV structure and function

Ten animals (VEH [n=5] and CBSC [n=5] –treated) were studied for 3Mons after IR/MI. Time dependent changes in cardiac structure and function were evaluated with ECHO and invasive hemodynamic measurements; which were performed before IR/MI and were repeated during terminal studies. ECHO measurements documented increases in LVEDV and LVESV in both treatment groups vs. baseline. However, CBSC–treated hearts showed significantly less progressive LV chamber dilation as compared to VEH–treated hearts. At 3Mons' post–MI, the LVEDV and LVESV of CBSC–treated animals were significantly

Author Manuscript Author Manuscript Author Manuscript Author Manuscript

smaller than in VEH–treated animals (Figure 5A & B) (LVEDV – [53.0 ± 3.0 ml vs. 43 ± 2.5 ml]; LVESV – [38.6 ± 3.4 ml vs. 22.0 ± 2.4 ml] $p \leq 0.05$). LVEF was reduced in both groups by about 10% at 1Mon post–MI (Figure 5C). Over the next 2Mon LVEF fell in the VEH–treated animals while EF remained stable in CBSC–treated animals. LVEF was significantly greater in CBSC– vs. VEH– treated animals at 3Mons' post–MI (Figure 5C). At 3Mons post-MI the SV and CO were both significantly reduced in the VEH–treated vs. CBSC–treated animals (Figure 5E & F). Accounting for the growth of the animals by normalizing to the body surface area (BSA–m^2), did not change the differences between treatment groups (Online Table IV). Chamber dilation was confirmed through structural measurements of the cardiac internal diameter at end-diastole and -systole (Figure 5H–K); also through a significant reduction in the LV relative wall thickness (Online Table IV). The intraventricular septum dimension was better preserved in CBSC-treated vs. VEH – treated animals (Figure 5G & J), while the internal diameter of the LV was significantly less dilated at 3Mons post-MI in CBCS-treated vs. VEH–treated animals (Figure 5H & K). These studies show that CBSC therapy reduces the progression of cardiac structural remodeling during the three months of study after MI.

CBSCs reduce hemodynamic deterioration and preserve contractile reserve

Differences in ventricular dilation at 3Mons' post–MI determined with serial ECHO were confirmed in terminal studies using invasive hemodynamic methods (Figure 6). The PV loops (Figure 6A) and end–diastolic pressure–volume relationship (EDPVR) (Figure 6B), at spontaneous heart rates, were shifted to significantly larger volumes at 3Mons' post–MI in the VEH–treated animals. This rightward shift of the PV relationships at end–diastole confirms ventricular dilation. Significantly smaller changes in these parameters were found in the CBSC–treated animals (Figure 6D & 6E). There was significantly less rightward shift in the EDPVR in CBSC– vs. VEH –treated animals at 3Mons' post–MI (Figure 6H). These results confirm that CBSC treatment reduces progressive ventricular dilation and preserves LVEF as compared with VEH treatment (Figure 6G & H, Online Table V). The volumes at dP/dt max. & min. where not significantly increased in the CBSC–treated animals, further documenting preservation of cardiac chamber size in CBSC–treated animals (Online Table V). Consistent with previous work[3] diastolic function was decreased post–MI. The isovolumic relaxation time constant (τ) was prolonged and the minimal rate of relaxation (dP/dt min.) was decreased in VEH– vs. baseline, while these measurements were not significantly different with CBSCs (Online Table V).

The rightward shift in the PV loop in VEH– treated animals is consistent with a decrease in cardiac systolic function (Figure 6C). The ESPVR, an indicator of systolic performance, is determined by two parameters: the end–systolic elastance (Ees) (i.e. slope) and the volume intercept (V_0). Changes in both determinants are considered to determine changes in cardiac systolic function (i.e. contractility)[36, 37]. The ESPVR was shifted rightward to a greater extent in VEH– vs. CBSC–treated animals after MI (Figure 6I). The Ees was reduced in both CBSC– and VEH– treated animals (5.63 ± 0.40 to 4.35 ± 0.41 [CBSC] and 5.04 ± 0.39 to 3.78 ± 0.47 [VEH], $p > 0.05$ [between groups 3Mon post-MI]). The volume intercept (V_0) was significantly increased only in the VEH–treated animals vs. baseline (Online Table V). These studies document a reduction of cardiac function in all MI animals, regardless of

Author Manuscript Author Manuscript Author Manuscript Author Manuscript

treatment, with better preservation of cardiac contractile properties in CBSC–treated animals.

Reduced inotropic reserve is a characteristic feature of the failing heart[38]. To explore the idea that CBSC treatment improves post–MI contractile reserve, cardiac hemodynamics were measured in VEH– and CBSC–treated MI animals before and after DOB (Figure 6J – I). DOB (2.5ug/kg/min.) caused a shift in the EDPVR towards baseline in CBSC–treated but not in VEH–treated animals (Figure 6J & K). DOB treatment, in the CBSC cohort, created a significant leftward shifted the ESPVR beyond baseline levels (Figure 6I) and caused a 2–fold increase in the Ees (4.35 ± 0.41 [3Mo post–MI + CBSCs] to 8.09 ± 0.71 [+ DOB], $p \leq 0.05$) and did not alter V_0 (Online Table V). These changes were significantly greater than in DOB–treated MI +VEH animals (Figure 6J – L, Online Table V, $p \leq 0.05$). DOB only caused a significant increase in Ees in CBSC–treated animals (Online Table V). There was also a significant reduction in Ves and an increased EF with CBSC treatment + DOB vs. VEH + DOB (Online Table V). Collectively these data show that CBSC treatment preserves basal contractility and systolic functional reserve.

CBSC treatment reduces scar size, inhibits hypertrophic remodeling and apoptosis

Heart weight and heart weight to body weight ratios were not different in VEH– and CBSC–treated hearts (Online Table II). However, scar size was significantly smaller in CBSC– vs. VEH–treated animals at 3Mons' post–MI (8.5 ± 2.2% vs 16.15 ± 1.85%, $p \leq 0.05$) (Figure 7A). In addition, anterior wall thickness was significantly greater in CBSC– vs. VEH–treated animals (Figure 7B & C). At the cellular level, myocyte cross-sectional area (CSA, μm^2) was significantly smaller in CBSC– vs. VEH– treated hearts (BDZ – [565.8 ± 2.9 μm^2 vs. 304 ± 1.1 μm^2, $p \leq 0.0001$]; RZ – [400.6 ± 2.4 μm^2 vs. 276.6 ± 1.2 μm^2, $p \leq 0.0001$]) (Figure 7D & F), with a rightward shift in the BDZ and RZ CSA histograms (Figure 7E & G). CBSC CSA was slightly but significantly greater than non-infarcted control animals (Figure 7D & F), but significantly smaller than VEH–treated MI myocytes. Myocyte nuclear density (MND) per mm^2 was evaluated in the BDZ and RZ. MND was significantly greater in the CBSC–treated vs. VEH–treated animals (933.8 ± 85.25 myocyte nuclei/mm^2 vs. 623.1 ± 48.32 myocyte nuclei/mm^2, $p \leq 0.05$) (Figure 7H & I) but not significantly different from non-infarcted controls. There was a significant reduction in $TUNEL^+$ non-myocytes (Figure 7J) and myocytes (Figure 7K) at 3Mons in animals who received CBSC treatment compared to VEH–treated animals in the BDZ and RZ. These data show that CBSC–treated hearts have greater muscle mass due to a reduction in scar with no different in HW or HW/BW ratio. CBSC–treated animals had smaller cardiac myocytes as observed by a significant reduction in CSA and significant increase in cardiac myocytes nuclei per mm^2 as compared to VEH–treated animals. Significantly reduced myocyte apoptosis over 3Mons may give insight into how there is more muscle mass, reduced scar and more myocytes per mm^2 as compared VEH–treated IR/MI hearts.

CBSCs induces myocyte proliferation with little recruitment of $ckit^+$ cells

EdU was infused into 3Mon VEH– and CBSC–treated animals (n=5, each) for the first 7 days after MI to identify cells that incorporate EdU into their DNA during this time period (Figure 8); EdU was also infused in non-infarcted controls (n=3) to observed baseline EdU

Author Manuscript Author Manuscript Author Manuscript Author Manuscript

incorporation. We imaged and quantified the number of EdU^+ cells at 3Mons' post–MI ± CBSCs and non-infarcted controls. Confocal images from the IZ, BDZ, RZ and sBDZ of all animals were examined (Figure 8A1–A4 [VEH] & B1–B4[CBSC]) and EdU^+ cells were identified and quantified[34]. We calculated the total number of nuclei ($DAPI^+$ [all cells]), $EdU^+/DAPI^+$ cells (total EdU^+ cells), $Actin^+/DAPI^+$ (total myocytes) and $EdU^+/Actin^+/DAPI^+$ cells (EdU^+ myocytes) (Figure 8 & Online Figure VIII A–D) in each tissue section. No GFP^+ cells were found in any 3Mon post–MI hearts, suggesting that none of the injected CBSCs were still present at this time point. The percentage of EdU^+ nuclei (Figure 8A1–A4 & B1–B4 [arrowheads]) was not different in CBSC– vs. VEH–treated heart in any region (Figure 8C1–C4). There was a significant increase in the total EdU^+ cells in both treatment arms when compared to non-infarcted controls in the IZ and BDZs. However, EdU^+ cardiac myocytes were easily identified in every heart (Figure 8A1–A4 and B1–B4 [arrows]) (Online Figure IX). None of these myocytes were GFP^+, so they were not derived from injected CBSCs. The percentage of EdU^+ myocytes out of total myocytes was significantly greater in CBSC hearts in all regions adjoining the MI and the majority of the EdU^+ myocytes were at or near the infarct BDZ (Figure 8B1–B4 [arrows] & 8D1–D4). In non-infarcted controls the percentage of EdU^+ myocytes was significantly reduced in the IZ (i.e AW) and both BDZs (i.e. LW & SW). The percentage of EdU^+ myocytes was not significantly increased in the areas of the heart that are remote from the infarct (Figure 8D3).

To explore whether recruitment of endogenous stem cell populations to the areas of exogenous stem cell injections occurred, we examined the number of $ckit^+$ stem cells near injection sites in all animals at 3Mons post-MI. Only a few $ckit^+$ cells were found (less than 0.01% of total nuclei in both groups). Representative images of $ckit^+$ cells found near the injection sites are in the online supplement (Online Figure X).

CBSC treatment induces vessel formation

To investigate the formation of new vessel we quantified the number of VWF^+ and VWF^+/SMA^+ vessel per mm^2. A significant increase in VWF^+ was found (vs. VEH) in CBSC–treated hearts and dual positive vessels were observed in the IZ (Online Figure XI A & E.) However, in most other regions of the heart there was no significant difference between groups (Online Figure XI B, D, F & H). Interestingly, there was a significant increase in the density of VWF^+ vessels in the RZ of VEH–treated animals vs. CBSCs (Online Figure XI C). Significant increases in vessel density in CBSC–treated animals' may be involved in the beneficial functional effects of CBSC treatment observed at 3Mons post-MI.

DISCUSSION

The present study was designed to test the safety and efficacy of transendocardial administration of CBSCs in a randomized, blinded, placebo controlled preclinical swine model of I/R induced MI. There were several major new findings. The studies performed showed that transendocardial injection of allogeneic CBSC is safe both acutely and chronically, giving no evidence of ectopic tissue formation or lethal arrhythmogenesis. CBSC retention within injection sites was shown at 72hrs post IR/MI and these CBSCs were

Author Manuscript Author Manuscript Author Manuscript Author Manuscript

EdU$^+$, consistent with the idea that they were proliferative after injection. CBSCs had no effect on IR/MI– induced myocyte necrosis or on initial infarct size. However, CBSC treatment reduced reactive fibrosis (scar size) at 3Mons' post IR/MI. Progressive structural pathological remodeling (i.e. hypertrophy of viable tissue, wall thinning within the scar and dilation of the LV chamber) was also reduced with allogeneic CBSC treatment. There was preservation of LV systolic and diastolic function and a greater cardiac functional reserve in the CBSC–treated animals. A small but significantly greater number of EdU$^+$ cardiac myocytes were found in CBSC–treated hearts 3Mons' post IR/MI. These studies strongly support the idea that delivery of CBSCs to the MI border zone in the immediate post IR/MI heart causes beneficial changes in post–MI remodeling that reduce adverse structural and functional derangements (Online Figure XII).

CBSCs are not cardioprotective but preserve intrinsic myocardial performance

The present experiments showed that IR/MI induced similar amounts of cardiac injury in CBSC– and VEH–treated animals. All IR/MI animals had similar increases in circulating troponin levels (Figure 2B & C). In addition, the amount of necrotic tissue identified with TTC staining at 3 days' post–MI was identical in both treatment groups. These results strongly support the idea that CBSCs do not provide cardio–protection, to reduce the initial infarct size, at least with the approaches employed in these experiments. However, we did not measure the potential effects of CBSC's on the area at risk (AAR), using Evan's blue staining. These data would give insight to amount of tissue that could be lost to infarct expansion over time, or rescued by CBSC therapy. Regardless, these results are not surprising since our IR/MI model causes necrotic cell death within the infarct core and an infarct border zone of uncoupled cardiac tissue, as we have shown previously[30]. Our results do suggest that CBSCs reduce infarct expansion, which would likely result from progressive death of those myocytes at the MI border zone that have uncoupled from the parent myocardium and have survived the necrotic cell death caused by IR/MI. TUNEL staining revealed a reduction in non-myocyte death 3 days' post MI and a trend towards a reduction in TUNEL$^+$ myocyte in the CBSC–treated group. Others have shown acute cardioprotective features of exosomes from cardiosphere–derived stem cells under similar experimental conditions[39]. One possible explanation for these differences is that our IR/MI model causes a large necrotic infarct core which develops within minutes upon reperfusion, whereas the damage in the previous report appears to produce an infarct with intact, non–necrotic myocytes with apoptotic myocyte death in the infarct core and border zones[39].

CBSC injections did not improve the echocardiographic determined cardiac volumes (EDV, ESV, LVEF) or structural dimensions at 72hrs, providing additional evidence that these cells did not provide immediate cardiac protection. However, myocardial performance, measured by LV longitudinal and radial strain, were better preserved in CBSC–treated animals. Speckle–tracking echocardiographic strain analysis is known to be more sensitive and identifies global and regional abnormalities in cardiac muscle contraction earlier than classical ECHO–derived volumetric measurements (i.e. LVEF)[40, 41]. The basis for these CBSC–mediated improvements in global strain in the absence of a cardio–protective effect are unclear at present but might be best explained by a wall stabilizing effect of injected CBSCs[29].

Author Manuscript Author Manuscript Author Manuscript Author Manuscript

CBSCs survive and expand during the first few days post IR/MI

GFP$^+$ CBSCs injected into the IR/MI border zone were found in every animal at 3 days' post IR/MI. EdU was infused for the 3 days and most CBSCs were also EdU$^+$, showing that a portion of the injected cells survive and proliferate over this period. We also found a large percentage of the nuclei in the injured regions of the heart were EdU$^+$ (about 20%), and the vast majority of these cells were nonmyocytes. The number of EdU$^+$ nonmyocytes in the damaged regions of the heart was increased in CBSC–treated animals. The identity of these proliferative cells was determined to primarily consist of VWF$^+$ cells, SMA$^+$ cells and CD45$^+$ cells confirming that post IR/MI, infiltrating cells are primarily from the circulation as well as myofibroblasts[42, 43]. The potential links between increases in proliferative nonmyocytes in CBSC–treated animals and the subsequent reduction in pathological post–MI remodeling needs to be defined.

CBSC therapy reduces post–MI structural and functional remodeling

The 3Mon post IR/MI studies explored CBSC effects on scar size, cardiac hypertrophy, progressive LV chamber remodeling, loss of contractility and functional reserve. Similar to our previous results in mouse MI models[29], CBSC treatment resulted in a reduction in scar size (Figure 7A – C). It is not entirely clear how CBSCs cause a reduced scar burden but modulation of the post IR/MI inflammatory response is likely to be involved[44], and represents a topic for future studies and a target for future translational experiments. An inhibition or reduction in low levels of myocyte apoptosis (Figure 7) over long periods of time post-MI may also be a contributing factor to the increased myocyte mass and reduced scar burden in CBSC-treated animals.

Ventricular chamber dilation is a hallmark feature of pathological post IR/MI remodeling[45]. The present study showed that while CBSCs did not prevent necrotic cell death in the immediate post–MI time frame, they significantly slowed the rate of and reduced the amount of ventricular remodeling as independently observed by ECHO and invasive hemodynamics studies.

Depression of cardiac systolic function with reduced contractile reserve is a classical feature of human heart failure[46]. The amount/extent of dysfunction is proportionate to the burden of the heart failure syndrome. The swine model of IR/MI captures early features of MI–induced heart failure. ECHO measurements showed progressive cardiac chamber dilation that was associated with progressive depression in cardiac systolic function (Figures 5 & 6 and Online Table IV). Our results also show a significant shift in ED– and ES–PVRs measured with invasive hemodynamic techniques (Figures 6A – C). Changes in the PV loops of 3Mon post–MI animals document cardiac chamber dilation and reduced basal cardiac function (Figure 6A – F). Cardiac contractile reserve, as measured by a DOB response, was also significantly reduced in VEH– vs. CBSC–treated MI animals. Collectively our studies show that CBSC treatment reduced post–MI structural remodeling and preserved post–MI cardiac systolic function and inotropic reserve (Figures 6G – I).

Our studies did not find evidence of allogeneic CBSC persistence or differentiation into new cardiac tissue (blood vessels or myocytes) at 3Mons post–MI. These results suggest that

Author Manuscript Author Manuscript Author Manuscript Author Manuscript

paracrine factors released from CBSCs over the first few days/weeks following IR/MI are responsible for reduced post–MI remodeling and improved cardiac pump function[28, 29]. CBSCs were alive and proliferative in vivo at 72hrs post–MI. Collectively our results suggest that CBSCs release factors that modify post IR/MI wound healing to reduce scar size and possibly limit myocyte death in the MI border zone in the weeks after MI, when infarcts size can expand[29, 47].

CBSC therapy increases muscle mass in the post–MI heart

The heart weight and HW/BW ratio of VEH– and CBSC–treated animals were not different 3Mons after MI (Online Table II), but scar mass was significantly smaller in CBSC–treated hearts, so muscle mass was greater in these hearts. Myocyte size was significantly smaller in CBSC– vs. VEH–treated hearts with greater MND per mm^2 within viable cardiac tissue (e.g. BDZ & RZ). In addition, there was significantly less cardiac myocyte apoptosis in CBSC– vs. VEH–treated hearts in the viable regions (e.g. BDZ & RZ) (Figure 7). These results, with simple, reliable techniques, strongly support the idea that there are more myocytes in the ventricles of CBSC–treated as compared to VEH–treated hearts. There are many possible reasons for the greater number of myocytes found in CBSC-treated hearts at 3 months post MI: (1) Progressive and chronic expansion of myocyte death in VEH–treated animals would leave these hearts with progressively fewer myocytes; while, (2) CBSCs might prevent the death of myocytes in the infarct BDZs, preserving myocyte number and leaving these hearts with more myocytes than the VEH-treated counterparts, and (3) CBSC treatment could induce new myocyte formation either through stimulation of endogenous myocyte division or recruitment of endogenous stem cells which then differentiate into new myocytes[48]. We are confident that there are more cardiac myocytes in the ventricles of CBSC-treated hearts (versus VEH-treated hearts) 3 mons post-MI. Both reduced myocyte death and enhanced myocyte regeneration were found at specific time periods. However, we cannot predict the overall contribution of these two processes to the greater myocyte number in CBSC-treated hearts since we did not measure them continuously, and we do not know the temporal nature of the two processes.

Our results suggest that CBSC treatment induces an increase in the number of newly formed myocytes within the first week post MI, particularly in the BDZs, and that these myocytes are derived from the host myocardium, not from recruitment of endogenous stem cell populations (Figures 8, Online Figure IX & X). Previous studies of post–MI cell therapy have reported a range of new myocyte formation from 1%[49] to ≥ 50%[50, 51], and the source of these new myocytes have been widely debated[49–53]. The current consensus in the field is that the normal adult heart has a very limited ability to form new myocytes, but that after injury there is a small but significant increase in new myocyte formation, with the new myocytes being derived primarily from preexisting myocytes[54–56]. Our data is consistent with these ideas and our previous in vitro study[28] suggests that the paracrine factors released from CBSCs could significantly enhance new myocyte formation. However, the number of EdU^+ myocytes identified is rather small (about 1.5% of the total myocytes counted) and EdU could be incorporated into cardiac myocytes that are not dividing[57]. Also, the number of EdU^+ myocytes observed (about 1.5% in the IZ and BDZs) in CBSC-treated hearts does not appear to be sufficient to explain the improved cardiac function. However, EdU labeling

Author Manuscript Author Manuscript Author Manuscript Author Manuscript

was only performed in the first week post–MI and new myocyte formation that occurred after the first week post MI would not be measured with our techniques. Multiple labeling periods could be used in future studies to address this issue. What is clear is that any newly formed myocytes were not derived from the injected CBSCs.

Study limitations

This study looked at a single stem cell type, delivered using one technique (direct intramuscular delivery) and at one dose and one-time point (immediate post–MI) in a small cohort of normal female pigs. The study showed significant CBSC benefits under the conditions tested. However, we recognize that our study was performed with a small sample size, so we are cautious with our conclusions. Future studies to translate these cells into a useful therapeutic would need to evaluate dose and time dependent effects and could include evaluations with magnetic resonance imaging with larger cohorts of animals. Mechanistic insights are almost always more limited in large animal studies. Investigating the area at risk (AAR) with Evan's blue staining would have helped confirm the potential for infarct expansion and any effects CBSC treatment may have had on the short- and long-term scar formation. Also, performing a study looking at EdU incorporation at different time points within the post-MI remodeling phase could help us understand the temporal nature of endogenous myocyte proliferation. However, we have used several independent, simple and reliable methods to show that CBSCs improve post–MI remodeling and do so through paracrine effect(s) leading to preserved cardiac structure and function.

Conclusions

Our experiments show that CBSCs delivered by transendocardial injection into the infarct border zone after IR/MI: (1) Cause no adverse effects, (2) survive and expand for at least 72hrs in the infarct border zone, (3) increase the number of proliferative cells in the injured heart after MI; (4) limit the progression of post–MI structural remodeling and (5) preserve cardiac pump function and contractile reserve. This is done through (6) inhibition of myocytes apoptosis chronically in the heart and (7) an increase in the number of EdU^+ cardiac myocytes. This leads to an increase in the total number of myocytes within the CBSC–treated hearts to be greater than in VEH–treated hearts. These findings support the idea that CBSC–therapy improves post–MI wound healing to reduce scar size, inhibit slow progression myocyte death, increase myocyte number and preserve cardiac function, limiting the progression towards HFrEF.

Supplementary Material

Refer to Web version on PubMed Central for supplementary material.

Acknowledgments

SOURCES OF FUNDING

This work was supported by the National Institute of Health, National Heart, Blood Lung Institute, Washington D.C. – Project Program Grant (5P01HL108806-04) (S.R.H.) and (1R56HL137850-01) (S.M.) The work is also supported by American Heart Association – Predoctoral Fellowship (14PRE20450006) (T.E.S. III) and Scientist Development Grant (S.M.).

Author Manuscript Author Manuscript Author Manuscript Author Manuscript

Nonstandard Abbreviations and Acronyms

AW/IZ	anterior wall/ infarct zone
CAD	Coronary artery disease
CBSCs	Cortical Bone Stem Cells
DOB	Dobutamine
EDPVR	End-diastolic Pressure-Volume Relationship
ESPVR	End-systolic Pressure-Volume Relationship
HFrEF	Heart failure with Reduced Ejection Fraction
LVEDV	Left Ventricular End-diastolic Volume
LVEF	Left Ventricular Ejection Fraction
LVESV	Left ventricular End-systolic Volume
LW/BDZ	lateral wall/ border zone
PW/RZ	posterior wall/ remote zone
SW/sBDZ	septal wall/ septal border zone
VEH	Vehicle

References

1. Vedanthan R, Seligman B, Fuster V. Global perspective on acute coronary syndrome: A burden on the young and poor. Circulation Research. 2014; 114:1959–1975. [PubMed: 24902978]
2. Lange RA, Hillis LD. Reperfusion therapy in acute myocardial infarction. N Engl J Med. 2002; 346:954–955. [PubMed: 11919303]
3. Lee S-T, White AJ, Matsushita S, Malliaras K, Steenbergen C, Zhang Y, Li T-S, Terrovitis J, Yee K, Simsir S, Makkar R, Marbán E. Intramyocardial injection of autologous cardiospheres or cardiosphere-derived cells preserves function and minimizes adverse ventricular remodeling in pigs with heart failure post-myocardial infarction. Journal of the American College of Cardiology. 2011; 57:455–465. [PubMed: 21251587]
4. Wang J, Zhang S, Rabinovich B, Bidaut L, Soghomonyan S, Alauddin MM, Bankson JA, Shpall E, Willerson JT, Gelovani JG, Yeh ET. Human cd34+ cells in experimental myocardial infarction: Long-term survival, sustained functional improvement, and mechanism of action. Circ Res. 2010; 106:1904–1911. [PubMed: 20448213]
5. Valina C, Pinkernell K, Song YH, Bai X, Sadat S, Campeau RJ, Le Jemtel TH, Alt E. Intracoronary administration of autologous adipose tissue-derived stem cells improves left ventricular function, perfusion, and remodelling after acute myocardial infarction. Eur Heart J. 2007; 28:2667–2677. [PubMed: 17933755]
6. Waksman R, Fournadjiev J, Baffour R, Pakala R, Hellinga D, Leborgne L, Yazdi H, Cheneau E, Wolfram R, Seabron R, Horton K, Kolodgie F, Virmani R, Rivera E. Transepicardial autologous bone marrow-derived mononuclear cell therapy in a porcine model of chronically infarcted myocardium. Cardiovasc Radiat Med. 2004; 5:125–131. [PubMed: 15721847]
7. Oskouei BN, Lamirault G, Joseph C, Treuer AV, Landa S, Da Silva J, Hatzistergos K, Dauer M, Balkan W, McNiece I, Hare JM. Increased potency of cardiac stem cells compared with bone

Author Manuscript Author Manuscript Author Manuscript Author Manuscript

marrow mesenchymal stem cells in cardiac repair. Stem Cells Transl Med. 2012; 1:116–124. [PubMed: 23197758]

8. Kubo H, Berretta RM, Jaleel N, Angert D, Houser SR. C-kit+ bone marrow stem cells differentiate into functional cardiac myocytes. Clin Transl Sci. 2009; 2:26–32. [PubMed: 20443864]
9. Ellison GM, Vicinanza C, Smith AJ, Aquila I, Leone A, Waring CD, Henning BJ, Stirparo GG, Papait R, Scarfo M, Agosti V, Viglietto G, Condorelli G, Indolfi C, Ottolenghi S, Torella D, Nadal-Ginard B. Adult c-kit(pos) cardiac stem cells are necessary and sufficient for functional cardiac regeneration and repair. Cell. 2013; 154:827–842. [PubMed: 23953114]
10. Smith RR, Barile L, Cho HC, Leppo MK, Hare JM, Messina E, Giacomello A, Abraham MR, Marbán E. Regenerative potential of cardiosphere-derived cells expanded from percutaneous endomyocardial biopsy specimens. Circulation. 2007; 115:896–908. [PubMed: 17283259]
11. Quevedo HC, Hatzistergos KE, Oskouei BN, Feigenbaum GS, Rodriguez JE, Valdes D, Pattany PM, Zambrano JP, Hu Q, McNiece I, Heldman AW, Hare JM. Allogeneic mesenchymal stem cells restore cardiac function in chronic ischemic cardiomyopathy via trilineage differentiating capacity. Proceedings of the National Academy of Sciences. 2009; 106:14022–14027.
12. Yoon YS, Wecker A, Heyd L, Park JS, Tkebuchava T, Kusano K, Hanley A, Scadova H, Qin G, Cha DH, Johnson KL, Aikawa R, Asahara T, Losordo DW. Clonally expanded novel multipotent stem cells from human bone marrow regenerate myocardium after myocardial infarction. J Clin Invest. 2005; 115:326–338. [PubMed: 15690083]
13. Li Q, Guo Y, Ou Q, Chen N, Wu WJ, Yuan F, O'Brien E, Wang T, Luo L, Hunt GN, Zhu X, Bolli R. Intracoronary administration of cardiac stem cells in mice: A new, improved technique for cell therapy in murine models. Basic Res Cardiol. 2011; 106:849–864. [PubMed: 21516491]
14. Cao F, Lin S, Xie X, Ray P, Patel M, Zhang X, Drukker M, Dylla SJ, Connolly AJ, Chen X, Weissman IL, Gambhir SS, Wu JC. In vivo visualization of embryonic stem cell survival, proliferation, and migration after cardiac delivery. Circulation. 2006; 113:1005–1014. [PubMed: 16476845]
15. Kinnaird T, Stabile E, Burnett MS, Shou M, Lee CW, Barr S, Fuchs S, Epstein SE. Local delivery of marrow-derived stromal cells augments collateral perfusion through paracrine mechanisms. Circulation. 2004; 109:1543–1549. [PubMed: 15023891]
16. Schuleri KH, Feigenbaum GS, Centola M, Weiss ES, Zimmet JM, Turney J, Kellner J, Zviman MM, Hatzistergos KE, Detrick B, Conte JV, McNiece I, Steenbergen C, Lardo AC, Hare JM. Autologous mesenchymal stem cells produce reverse remodelling in chronic ischaemic cardiomyopathy. Eur Heart J. 2009; 30:2722–2732. [PubMed: 19586959]
17. Ly HQ, Hoshino K, Pomerantseva I, Kawase Y, Yoneyama R, Takewa Y, Fortier A, Gibbs-Strauss SL, Vooght C, Frangioni JV, Hajjar RJ. In vivo myocardial distribution of multipotent progenitor cells following intracoronary delivery in a swine model of myocardial infarction. Eur Heart J. 2009; 30:2861–2868. [PubMed: 19687154]
18. Johnston PV, Sasano T, Mills K, Evers R, Lee ST, Smith RR, Lardo AC, Lai S, Steenbergen C, Gerstenblith G, Lange R, Marban E. Engraftment, differentiation, and functional benefits of autologous cardiosphere-derived cells in porcine ischemic cardiomyopathy. Circulation. 2009; 120:1075–1083. 1077 p following 1083. [PubMed: 19738142]
19. Heldman AW, DiFede DL, Fishman JE, Zambrano JP, Trachtenberg BH, Karantalis V, Mushtaq M, Williams AR, Suncion VY, McNiece IK, Ghersin E, Soto V, Lopera G, Miki R, Willens H, Hendel R, Mitrani R, Pattany P, Feigenbaum G, Oskouei B, Byrnes J, Lowery MH, Sierra J, Pujol MV, Delgado C, Gonzalez PJ, Rodriguez JE, Bagno LL, Rouy D, Altman P, Foo CW, da Silva J, Anderson E, Schwarz R, Mendizabal A, Hare JM. Transendocardial mesenchymal stem cells and mononuclear bone marrow cells for ischemic cardiomyopathy: The tac-hft randomized trial. Jama. 2014; 311:62–73. [PubMed: 24247587]
20. Vrtovec B, Poglajen G, Lezaic L, Sever M, Socan A, Domanovic D, Cernelc P, Torre-Amione G, Haddad F, Wu JC. Comparison of transendocardial and intracoronary cd34+ cell transplantation in patients with nonischemic dilated cardiomyopathy. Circulation. 2013; 128:S42–49. [PubMed: 24030420]
21. Makkar RR, Smith RR, Cheng K, Malliaras K, Thomson LE, Berman D, Czer LS, Marban L, Mendizabal A, Johnston PV, Russell SD, Schuleri KH, Lardo AC, Gerstenblith G, Marban E. Intracoronary cardiosphere-derived cells for heart regeneration after myocardial infarction

Author Manuscript Author Manuscript Author Manuscript Author Manuscript

(caduceus): A prospective, randomised phase 1 trial. Lancet. 2012; 379:895–904. [PubMed: 22336189]

22. Bolli R, Chugh AR, D'Amario D, Loughran JH, Stoddard MF, Ikram S, Beache GM, Wagner SG, Leri A, Hosoda T, Sanada F, Elmore JB, Goichberg P, Cappetta D, Solankhi NK, Fahsah I, Rokosh DG, Slaughter MS, Kajstura J, Anversa P. Cardiac stem cells in patients with ischaemic cardiomyopathy (scipio): Initial results of a randomised phase 1 trial. Lancet. 2011; 378:1847–1857. [PubMed: 22088800]
23. Quyyumi AA, Vasquez A, Kereiakes DJ, Klapholz M, Schaer GL, Abdel-Latif A, Frohwein S, Henry TD, Schatz RA, Dib N, Toma C, Davidson CJ, Barsness GW, Shavelle DM, Cohen M, Poole J, Moss T, Hyde P, Kanakaraj AM, Druker V, Chung A, Junge C, Preti RA, Smith RL, Mazzo DJ, Pecora A, Losordo DW. Preserve-ami: A randomized, double-blind, placebo-controlled clinical trial of intracoronary administration of autologous cd34+ cells in patients with left ventricular dysfunction post stemi. Circ Res. 2017; 120:324–331. [PubMed: 27821724]
24. Schachinger V, Erbs S, Elsasser A, Haberbosch W, Hambrecht R, Holschermann H, Yu J, Corti R, Mathey DG, Hamm CW, Suselbeck T, Werner N, Haase J, Neuzner J, Germing A, Mark B, Assmus B, Tonn T, Dimmeler S, Zeiher AM. Improved clinical outcome after intracoronary administration of bone-marrow-derived progenitor cells in acute myocardial infarction: Final 1-year results of the repair-ami trial. Eur Heart J. 2006; 27:2775–2783. [PubMed: 17098754]
25. Assmus B, Schachinger V, Teupe C, Britten M, Lehmann R, Dobert N, Grunwald F, Aicher A, Urbich C, Martin H, Hoelzer D, Dimmeler S, Zeiher AM. Transplantation of progenitor cells and regeneration enhancement in acute myocardial infarction (topcare-ami). Circulation. 2002; 106:3009–3017. [PubMed: 12473544]
26. Williams AR, Suncion VY, McCall F, Guerra D, Mather J, Zambrano JP, Heldman AW, Hare JM. Durable scar size reduction due to allogeneic mesenchymal stem cell therapy regulates whole-chamber remodeling. J Am Heart Assoc. 2013; 2:000140.
27. Hare JM, DiFede DL, Rieger AC, Florea V, Landin AM, El-Khorazaty J, Khan A, Mushtaq M, Lowery MH, Byrnes JJ, Hendel RC, Cohen MG, Alfonso CE, Valasaki K, Pujol MV, Golpanian S, Ghersin E, Fishman JE, Pattany P, Gomes SA, Delgado C, Miki R, Abuzeid F, Vidro-Casiano M, Premer C, Medina A, Porras V, Hatzistergos KE, Anderson E, Mendizabal A, Mitrani R, Heldman AW. Randomized comparison of allogeneic versus autologous mesenchymal stem cells for nonischemic dilated cardiomyopathy: Poseidon-dcm trial. J Am Coll Cardiol. 2017; 69:526–537. [PubMed: 27856208]
28. Mohsin S, Troupes CD, Starosta T, Sharp TE, Agra EJ, Smith SC, Duran JM, Zalavadia N, Zhou Y, Kubo H, Berretta RM, Houser SR. Unique features of cortical bone stem cells associated with repair of the injured heart. Circ Res. 2015; 15:307362.
29. Duran JM, Makarewich CA, Sharp TE, Starosta T, Zhu F, Hoffman NE, Chiba Y, Madesh M, Berretta RM, Kubo H, Houser SR. Bone-derived stem cells repair the heart after myocardial infarction through transdifferentiation and paracrine signaling mechanisms. Circulation Research. 2013; 113:539–552. [PubMed: 23801066]
30. Duran JM, Taghavi S, Berretta RM, Makarewich CA, Sharp T Iii, Starosta T, Udeshi F, George JC, Kubo H, Houser SR. A characterization and targeting of the infarct border zone in a swine model of myocardial infarction. Clinical and Translational Science. 2012; 5:416–421. [PubMed: 23067355]
31. Bolli R, Tang X-L, Sanganalmath SK, Rimoldi O, Mosna F, Abdel-Latif A, Jneid H, Rota M, Leri A, Kajstura J. Intracoronary delivery of autologous cardiac stem cells improves cardiac function in a porcine model of chronic ischemic cardiomyopathy. Circulation. 2013; 128doi: 10.1161/CIRCULATIONAHA.1112.001075
32. Kajstura J, Rota M, Whang B, Cascapera S, Hosoda T, Bearzi C, Nurzynska D, Kasahara H, Zias E, Bonafe M, Nadal-Ginard B, Torella D, Nascimbene A, Quaini F, Urbanek K, Leri A, Anversa P. Bone marrow cells differentiate in cardiac cell lineages after infarction independently of cell fusion. Circ Res. 2005; 96:127–137. [PubMed: 15569828]
33. Orlic D, Kajstura J, Chimenti S, Jakoniuk I, Anderson SM, Li B, Pickel J, McKay R, Nadal-Ginard B, Bodine DM, Leri A, Anversa P. Bone marrow cells regenerate infarcted myocardium. Nature. 2001; 410:701–705. [PubMed: 11287958]

Author Manuscript Author Manuscript Author Manuscript Author Manuscript

34. Gross P, Honnorat N, Varol E, Wallner M, Trappanese DM, Sharp TE, Starosta T, Duran JM, Koller S, Davatzikos C, Houser SR. Nuquantus: Machine learning software for the characterization and quantification of cell nuclei in complex immunofluorescent tissue images. Sci Rep. 2016; 6:23431. [PubMed: 27005843]
35. Stewart S, Winters GL, Fishbein MC, Tazelaar HD, Kobashigawa J, Abrams J, Andersen CB, Angelini A, Berry GJ, Burke MM, Demetris AJ, Hammond E, Itescu S, Marboe CC, McManus B, Reed EF, Reinsmoen NL, Rodriguez ER, Rose AG, Rose M, Suciu-Focia N, Zeevi A, Billingham ME. Revision of the 1990 working formulation for the standardization of nomenclature in the diagnosis of heart rejection. J Heart Lung Transplant. 2005; 24:1710–1720. [PubMed: 16297770]
36. Burkhoff D, Mirsky I, Suga H. Assessment of systolic and diastolic ventricular properties via pressure-volume analysis: A guide for clinical, translational, and basic researchers. Am J Physiol Heart Circ Physiol. 2005; 289:H501–512. [PubMed: 16014610]
37. Alogna A, Manninger M, Schwarzl M, Zirngast B, Steendijk P, Verderber J, Zweiker D, Maechler H, Pieske BM, Post H. Inotropic effects of experimental hyperthermia and hypothermia on left ventricular function in pigs-comparison with dobutamine. Critical care medicine. 2016; 44:e158–167. [PubMed: 26474110]
38. El-Armouche A, Eschenhagen T. Beta-adrenergic stimulation and myocardial function in the failing heart. Heart Fail Rev. 2009; 14:225–241. [PubMed: 19110970]
39. Gallet R, Dawkins J, Valle J, Simsolo E, de Couto G, Middleton R, Tseliou E, Luthringer D, Kreke M, Smith RR, Marban L, Ghaleh B, Marban E. Exosomes secreted by cardiosphere-derived cells reduce scarring, attenuate adverse remodelling, and improve function in acute and chronic porcine myocardial infarction. Eur Heart J. 2017; 38:201–211. [PubMed: 28158410]
40. Bauer M, Cheng S, Jain M, Ngoy S, Theodoropoulos C, Trujillo A, Lin FC, Liao R. Echocardiographic speckle-tracking based strain imaging for rapid cardiovascular phenotyping in mice. Circ Res. 2011; 108:908–916. [PubMed: 21372284]
41. Stanton T, Leano R, Marwick TH. Prediction of all-cause mortality from global longitudinal speckle strain: Comparison with ejection fraction and wall motion scoring. Circ Cardiovasc Imaging. 2009; 2:356–364. [PubMed: 19808623]
42. Frangogiannis NG. Regulation of the inflammatory response in cardiac repair. Circulation Research. 2012; 110:159–173. [PubMed: 22223212]
43. Marchant DJ, Boyd JH, Lin DC, Granville DJ, Garmaroudi FS, McManus BM. Inflammation in myocardial diseases. Circulation Research. 2012; 110:126–144. [PubMed: 22223210]
44. Karantalis V, Hare JM. Use of mesenchymal stem cells for therapy of cardiac disease. Circulation Research. 2015; 116:1413–1430. [PubMed: 25858066]
45. Pfeffer MA, Braunwald E. Ventricular remodeling after myocardial infarction. Experimental observations and clinical implications. Circulation. 1990; 81:1161–1172. [PubMed: 2138525]
46. Braunwald E. Heart failure. JACC: Heart Failure. 2013; 1:1–20. [PubMed: 24621794]
47. Richardson WJ, Holmes JW. Why is infarct expansion such an elusive therapeutic target? Journal of cardiovascular translational research. 2015; 8:421–430. [PubMed: 26390882]
48. Hatzistergos KE, Quevedo H, Oskouei BN, Hu Q, Feigenbaum GS, Margitich IS, Mazhari R, Boyle AJ, Zambrano JP, Rodriguez JE, Dulce R, Pattany PM, Valdes D, Revilla C, Heldman AW, McNiece I, Hare JM. Bone marrow mesenchymal stem cells stimulate cardiac stem cell proliferation and differentiation. Circ Res. 2010; 107:913–922. [PubMed: 20671238]
49. Yoon, Y-s, Wecker, A., Heyd, L., Park, J-S., Tkebuchava, T., Kusano, K., Hanley, A., Scadova, H., Qin, G., Cha, D-H., Johnson, KL., Aikawa, R., Asahara, T., Losordo, DW. Clonally expanded novel multipotent stem cells from human bone marrow regenerate myocardium after myocardial infarction. Journal of Clinical Investigation. 2005; 115:326–338. [PubMed: 15690083]
50. Beltrami AP, Barlucchi L, Torella D, Baker M, Limana F, Chimenti S, Kasahara H, Rota M, Musso E, Urbanek K, Leri A, Kajstura J, Nadal-Ginard B, Anversa P. Adult cardiac stem cells are multipotent and support myocardial regeneration. Cell. 2003; 114:763–776. [PubMed: 14505575]
51. Oh H, Bradfute SB, Gallardo TD, Nakamura T, Gaussin V, Mishina Y, Pocius J, Michael LH, Behringer RR, Garry DJ, Entman ML, Schneider MD. Cardiac progenitor cells from adult myocardium: Homing, differentiation, and fusion after infarction. Proc Natl Acad Sci U S A. 2003; 100:12313–12318. [PubMed: 14530411]

Author Manuscript Author Manuscript Author Manuscript Author Manuscript

52. Hsieh PC, Segers VF, Davis ME, MacGillivray C, Gannon J, Molkentin JD, Robbins J, Lee RT. Evidence from a genetic fate-mapping study that stem cells refresh adult mammalian cardiomyocytes after injury. Nat Med. 2007; 13:970–974. [PubMed: 17660827]

53. Angert D, Berretta RM, Kubo H, Zhang H, Chen X, Wang W, Ogorek B, Barbe M, Houser SR. Repair of the injured adult heart involves new myocytes potentially derived from resident cardiac stem cells. Circ Res. 2011; 108:1226–1237. [PubMed: 21454756]

54. Senyo SE, Steinhauser ML, Pizzimenti CL, Yang VK, Cai L, Wang M, Wu TD, Guerquin-Kern JL, Lechene CP, Lee RT. Mammalian heart renewal by pre-existing cardiomyocytes. Nature. 2013; 493:433–436. [PubMed: 23222518]

55. Ali SR, Hippenmeyer S, Saadat LV, Luo L, Weissman IL, Ardehali R. Existing cardiomyocytes generate cardiomyocytes at a low rate after birth in mice. Proceedings of the National Academy of Sciences of the United States of America. 2014; 111:8850–8855. [PubMed: 24876275]

56. Beltrami AP, Urbanek K, Kajstura J, Yan SM, Finato N, Bussani R, Nadal-Ginard B, Silvestri F, Leri A, Beltrami CA, Anversa P. Evidence that human cardiac myocytes divide after myocardial infarction. N Engl J Med. 2001; 344:1750–1757. [PubMed: 11396441]

57. Grabner W, Pfitzer P. Number of nuclei in isolated myocardial cells of pigs. Virchows Arch B Cell Pathol. 1974; 15:279–294. [PubMed: 4135954]

Author Manuscript Author Manuscript Author Manuscript Author Manuscript

NOVELTY AND SIGNIFICANCE

What Is Known?

- Ischemia-reperfusion myocardial infarction (IR/MI) leads to scar formation within the infarct zone, pathological remodeling of remaining viable myocardium, and LV chamber dilation leading to cardiac dysfunction which is hallmarked by a reduced left ventricular ejection fraction (LVEF).
- Cortical Bone Stem Cells (CBSCs) are unique from mesenchymal and cardiac derived stem cells (MSC & CDCs) and may be superior in their ability to repair the heart post-MI.

What New Information Does This Article Contribute?

- This is the first translational large animal study performed utilizing CBSCs.
- Allogeneic transendocardial delivery of CBSCs acutely post-MI is safe and efficacious, permitting cell retention for at least 3 days.
- CBSC therapy alters the progression of pathological remodeling by increasing the number of proliferative cells at 3 days, reducing scar size through a reduction in myocyte apoptosis and an increase in endogenous myocytes proliferation at 3 months post-MI. This inhibition of pathological remodeling leads to preservation of cardiac structure and functional reserve.

Mesenchymal and cardiac stem cells have been studied over the last several decades as therapeutic strategies in the post-MI and heart failure settings. While proven to be safe in patients, these cell types have shown very modest improvements in functional and survival outcomes leading to the need for the investigation of novel cell and cell-based therapies. We identified a novel stem cell population derived from the cortical bone (CBSCs). Previously, we performed in vitro and in vivo studies comparing CBSC to more well-established cell-therapeutics (MSCs and CDCs). This present study is the first preclinical large animal study to investigate the safety, efficacy, and ultimately, the translational application of this cell type. We observed a change in the pathological remodeling that is classically seen post-MI. There was reduced scar size, less reactive myocyte growth within viable tissue, reduced myocyte cell death, an increase in the number of myocytes, and increase in the number of myocytes that had proliferated with CBSC versus vehicle treatment. This alteration of classical pathological remodeling lead to preserved cardiac structure and function over time. Moreover, a hallmark of the progression towards heart failure (HF) is a lack on systolic functional reserve, which was preserved with CBSC treatment when compared to vehicle treatment. These findings together demonstrate the safety and efficacy of CBSCs as a novel stem cell therapy in a preclinical large animal model and will be the foundation of future studies investigating dosing, time of delivery and comparison to standard of care.

Author Manuscript Author Manuscript Author Manuscript Author Manuscript

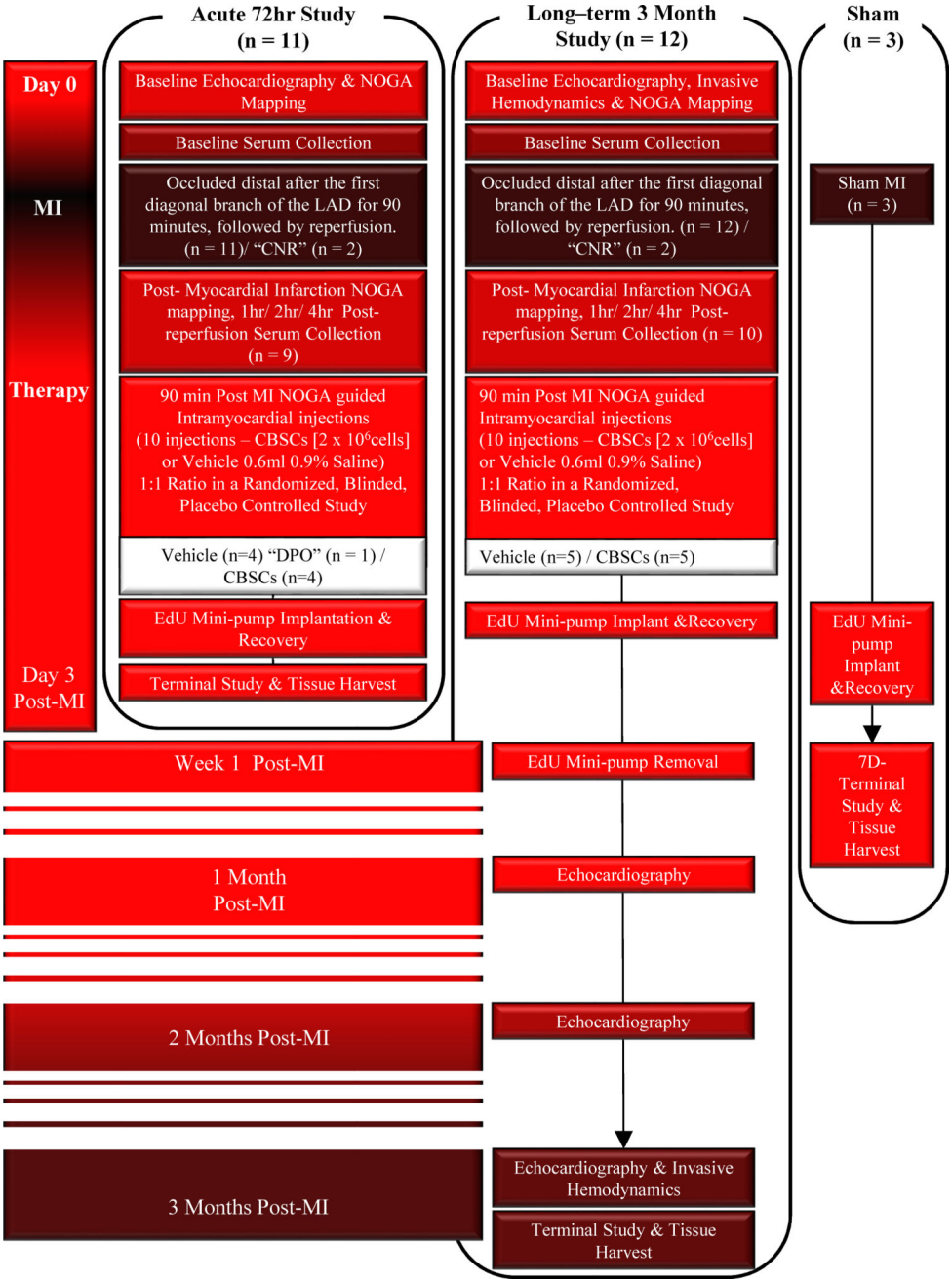

Figure 1. Study Timeline

Protocol used to perform baseline assessment, induce acute myocardial infarction, therapeutic delivery, EdU minipump implantation and explant, and functionally measurements.

Author Manuscript Author Manuscript Author Manuscript Author Manuscript

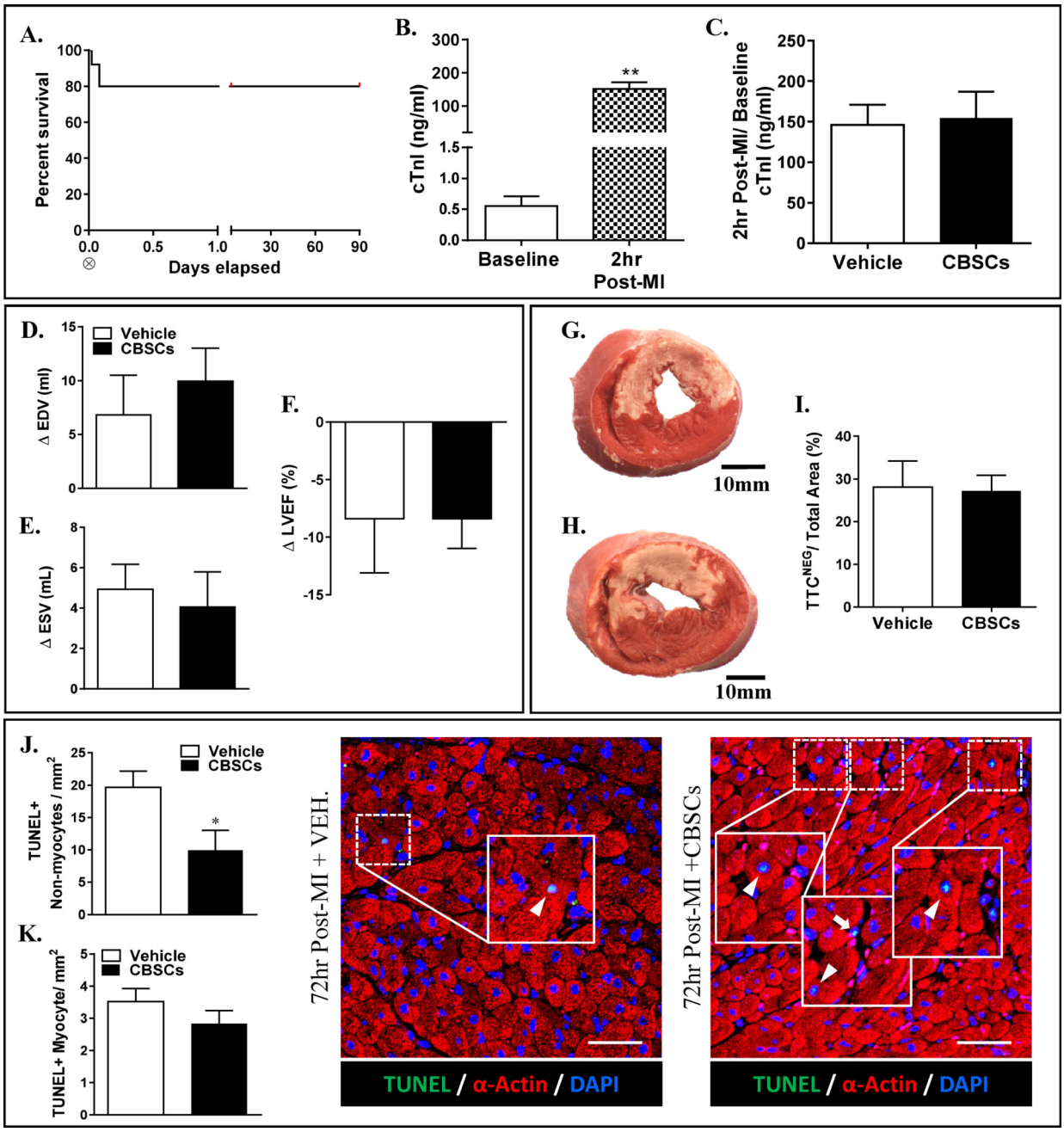

Figure 2. Survival and Initial Injury Assessment

Hematological, structural, and histological assessment of initial injury were performed at 72hrs post IR/MI. **(A.)** Survival curve of all twenty-three animals put on study. Two animals died during the ischemic period and one during the first 24hrs post-op. Eighteen survived and completed the study timeline. [X] = time of MI **(B.)** Circulating cardiac troponin I (cTnI) was analyzed at 2hrs post reperfusion in all animals (n = 18) p-value [**] ≤ 0.01 vs. baseline. **(C.)** The mean circulating cTnI at 2hrs post reperfusion between treatment groups. **(D.–F)** The change in left ventricular end-diastolic (EDV)/systolic (ESV) volume and ejection fraction (LVEF) in each treatment group at 72hrs post IR/MI. **(G. & H.)**

Author Manuscript Author Manuscript Author Manuscript Author Manuscript

Representative images of mid-myocardial cross-sections stained for TTC (VEH and CBSC, respectively). Scale Bar = 10mm. **(F.)** The mean TTC^{NEG} tissue (non-metabolically active tissue) as a percentage of total ventricular area. (n=4, each) **(J.)** The mean $TUNEL^{+}$ non-myocytes per mm^2 in each group. **(K.)** The mean $TUNEL^{+}$ myocytes per mm^2 in each group. Representative confocal images of $TUNEL^{+}$ myocytes (arrowheads) and non-myocytes (arrows) in VEH– and CBSC–treated animals at 72hrs post-MI. Scale bar = 50μm. p-value [*] ≤ 0.05 vs. VEH-treated. [**] ≤ 0.01 vs. baseline.

Author Manuscript Author Manuscript Author Manuscript Author Manuscript

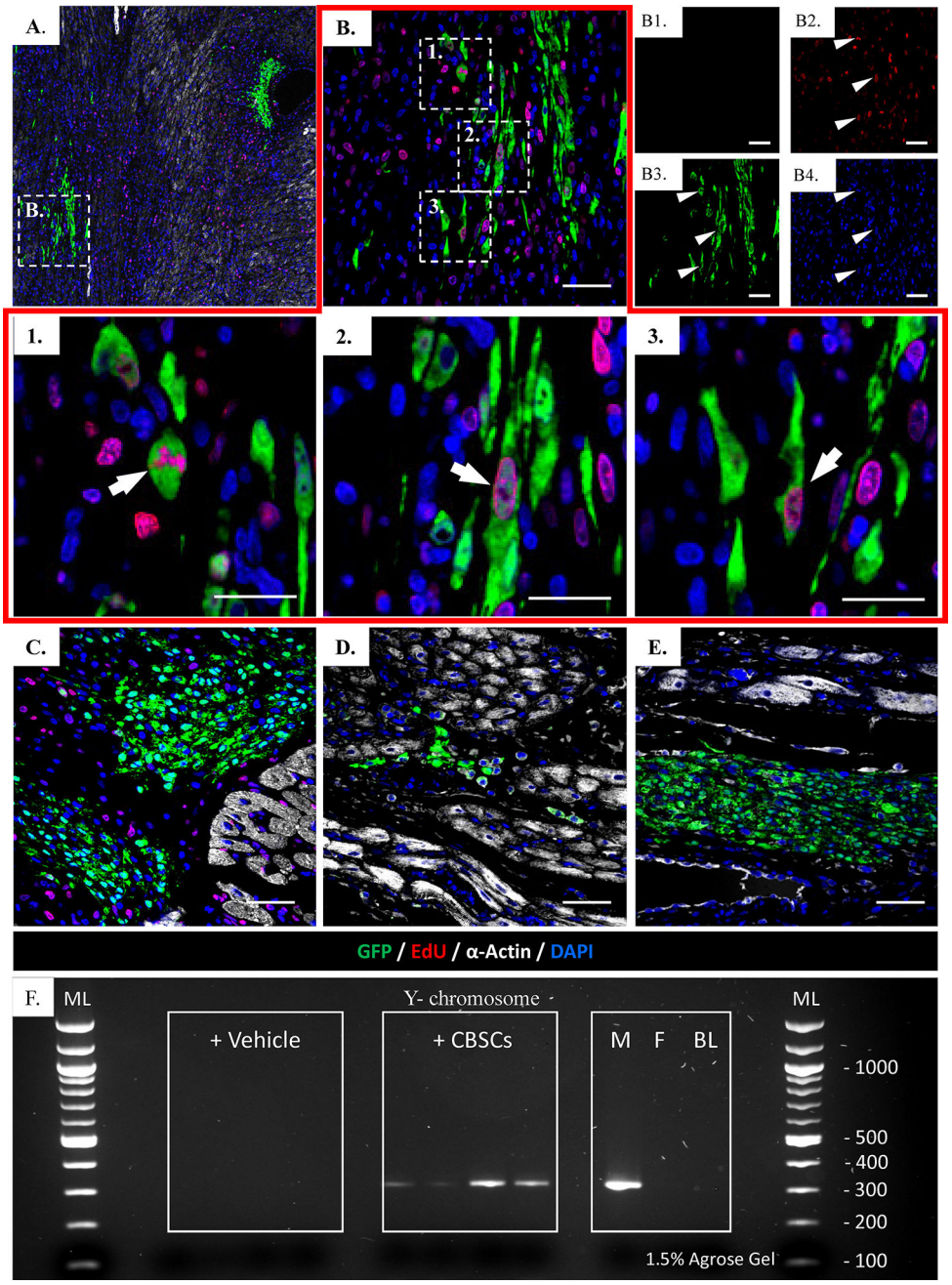

Figure 3. CBSC Retention and Proliferation

GFP^+/Y–chromosome$^+$ CBSC retention was assessed by immunofluorescence and PCR at 72hrs post IR/MI (n=4). **(A.)** Confocal image (10×) of a transendocardial injection site with GFP^+ CBSCs. **(B.)** Confocal image (40×) from injection site with GFP^+/EdU^+ CBSCs from image (A). **(B1. –B4.)** Single channels breakdown from 40× images (α-sarcomeric actin, EdU, GFP and DAPI, respectively) (arrowheads identify GFP^+/EdU^+ cells). **(1. – 3.)** Zoomed confocal images from the 40× image (B) of representative GFP^+/EdU^+ CBSCs (arrows). **(C.– E.)** Representative confocal images (40×) of GFP^+/EdU^+ CBSCs from animals 2–4. GFP (green), EdU (red), α-Actin (white) and DAPI (blue). Scale bars = 50μm

Author Manuscript Author Manuscript Author Manuscript Author Manuscript

(F.) PCR products run on 1.5% agrose gel from VEH and CBSC injection sites. BL = blank, F (– Control) = female heart, M (+ Control) = male heart, ML = molecular weight ladder. Product size ~ 300bp.

Author Manuscript Author Manuscript Author Manuscript Author Manuscript

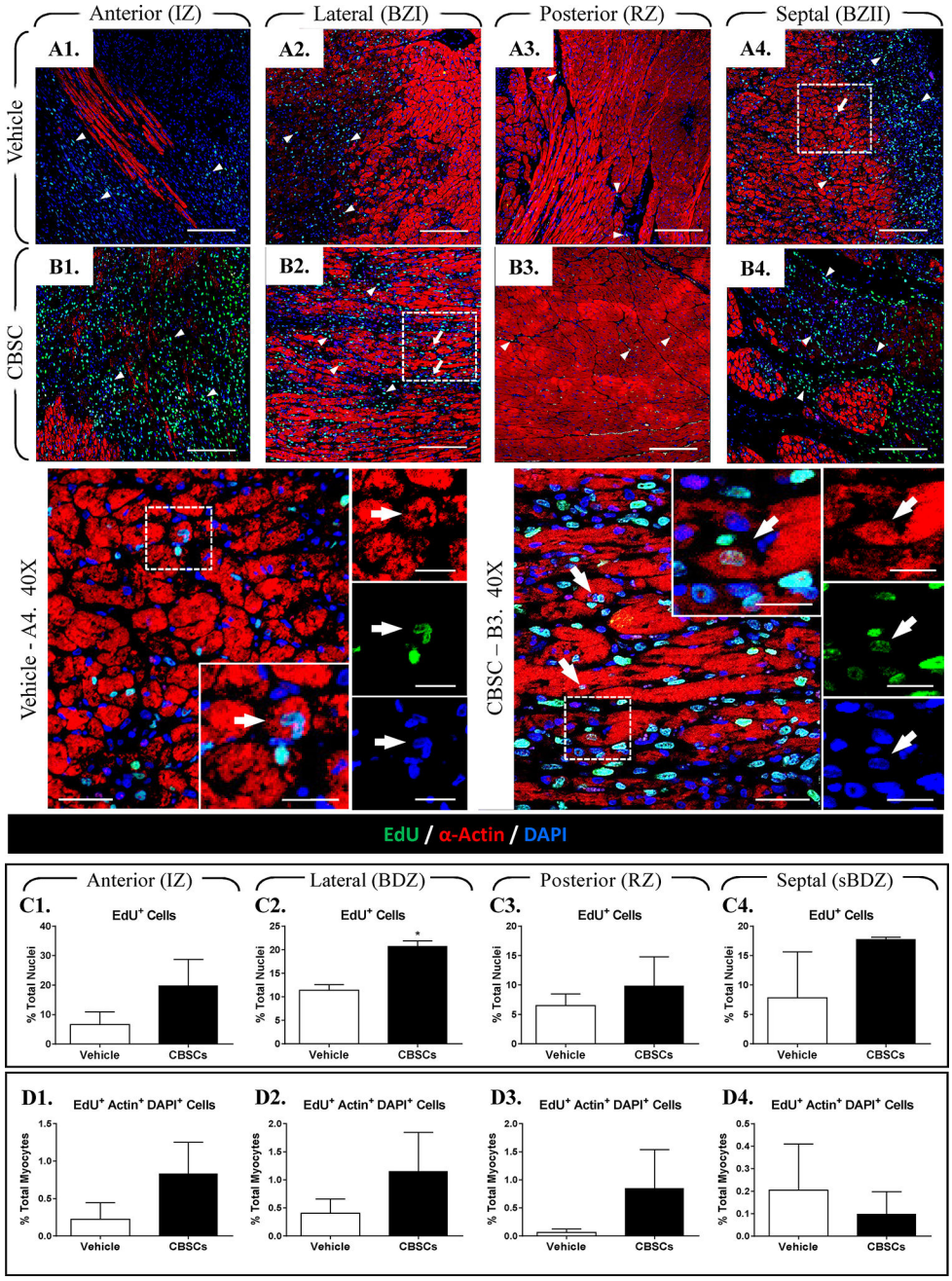

Figure 4. BSCs Induce an Increase in Proliferative Non–myocytes in the MI Border Zone EdU$^+$ cells were imaged and quantified at 72hrs post–MI in **(A)** VEH– and **(B)** CBSC–treated heart. **(A1. –A4.)** Representative confocal images (20×) from the four distinct regions of the myocardium post IR/MI + VEH. **(B1. –B4.)** Representative confocal images (20×) from the four distinct regions of the myocardium post IR/MI + CBSCs. 40× representative confocal images illustrates EdU$^+$ myocytes and non-myocytes from hearts ± CBSCs. EdU (green), α-Actin (red) and DAPI (blue). Arrows = myocytes, arrowheads = non–myocytes. 20× scale bars = 200μm, 40× scale bars = 50μm and zoom/channel breakdown scale bars = 25μm. **(C1. – C4.)** Quantification of total EdU$^+$ cells as a percentage of total DAPI$^+$ in each region. **(D1.**

Author Manuscript Author Manuscript Author Manuscript Author Manuscript

– D4.) Quantification of total $EdU^+Actin^+DAPI^+$ cells as a percentage of total $Actin^+DAPI^+$ (myocyte) in each region. N = 3, each group (*) p-value ≤ 0.05 vs. VEH.

Author Manuscript Author Manuscript Author Manuscript Author Manuscript

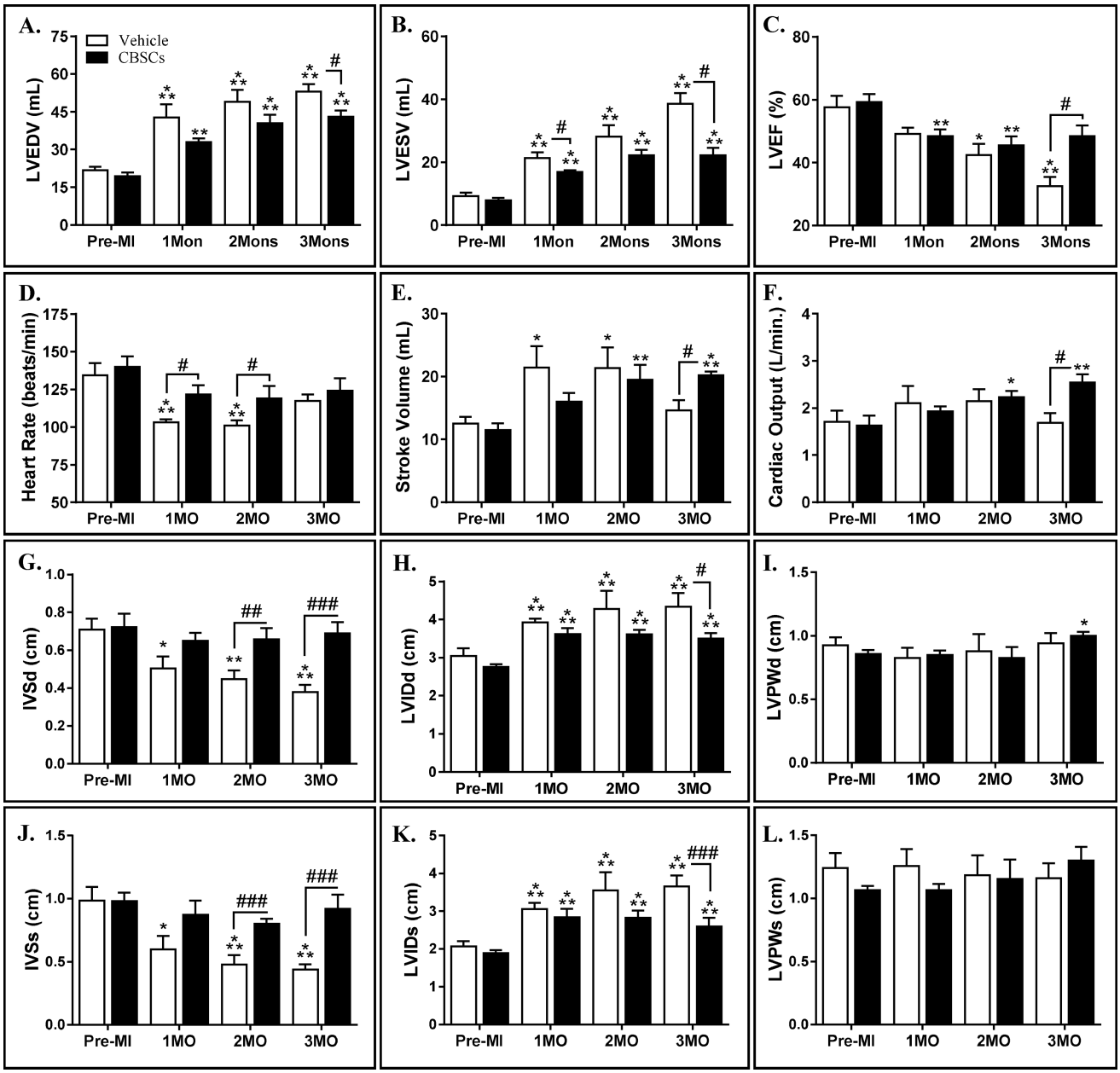

Figure 5. CBSCs Reduce Left Ventricular Structural Remodeling and Preserve Function Post IR/MI

Serial transthoracic echocardiography was performed. Volumetric measurements were assessed **(A.)** Left ventricular end-diastolic (LVEDV) and **(B.)** left ventricular end-systolic volumes (LVESV). **(C.)** Assessment of left ventricular ejection fraction (LVEF). **(D.)** Heart rate **(E.)** Stroke Volume **(F.)** Cardiac Output **(G.–I)** 2D m-mode LV wall thickness and internal diameter at end-diastole. **(J.–L.)** 2D m-mode LV wall thickness and internal diameter at end- systole. n = 5 in each group. P–value [*] ≤ 0.05, [**] ≤ 0.01 and [***] ≤ 0.005 vs. baseline within group, [#] ≤ 0.05, [##] ≤ 0.01 and [###] ≤ 0.005 vs. VEH. post–MI.

Author Manuscript Author Manuscript Author Manuscript Author Manuscript

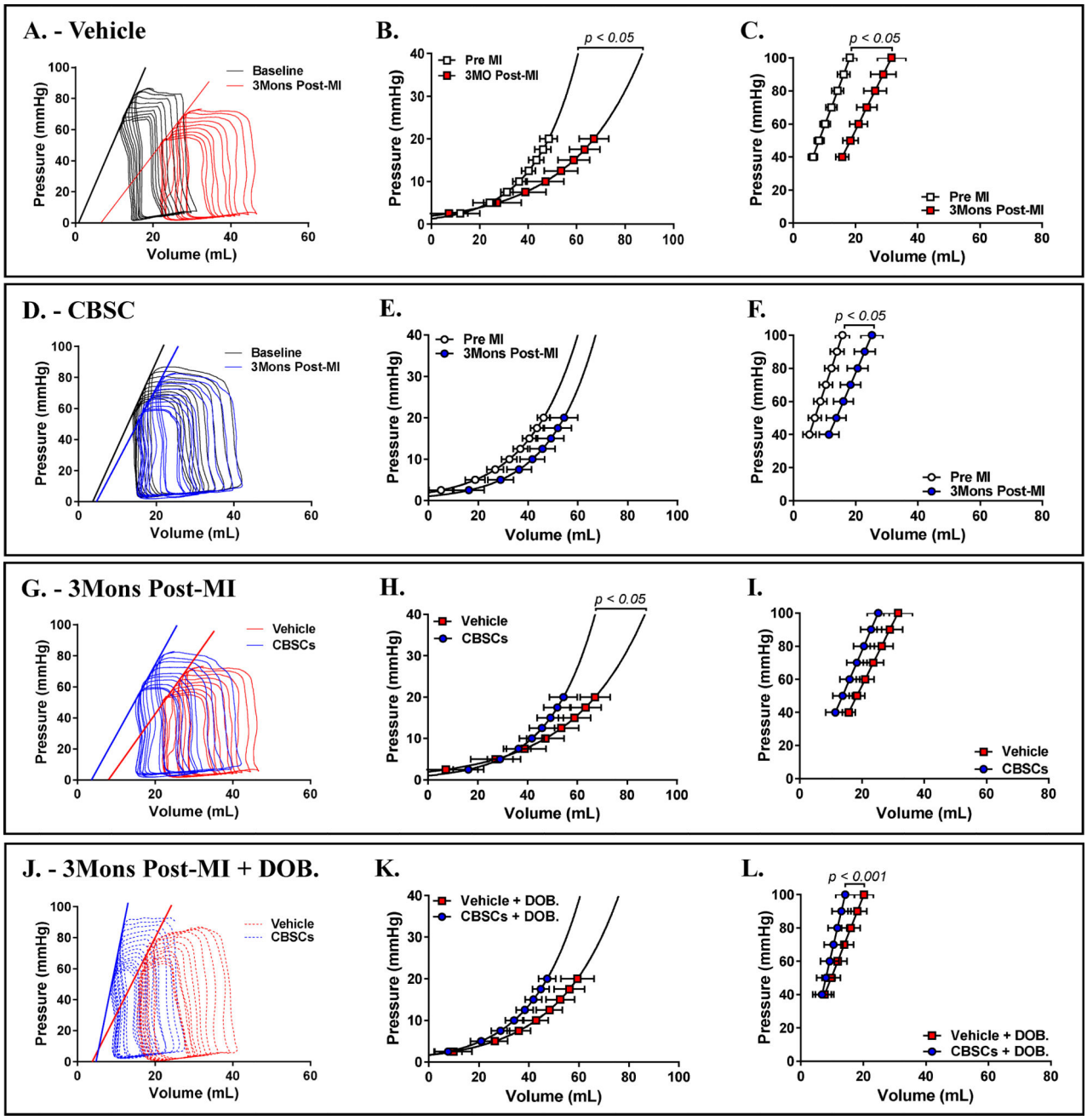

Figure 6. CBSCs Reduce Left Ventricular Dilation and Preserve Cardiac Functional Reserve

Invasive hemodynamics were performed at baseline and 3Mons' post–MI ± CBSCs ± DOB. **(A.)** Representative pressure volume (PV) loops at baseline and 3Mons' post–MI (red line) in VEH–treated animal. **(B. & C.)** EDPVR and ESPVR is shifted rightward 3Mons post–MI vs. pre–MI in VEH–treated animals. Pre–MI = open squares, 3Mons post–MI = red squares **(D.)** Representative PV loops from a CBSC–treated animal at baseline and 3Mons post–MI (blue line). **(E.)** EDPVR remains unchanged while **(F.)** ESPVR is shifted rightward 3Mo post–MI vs. pre–MI in CBSC–treated animals. Pre–MI = open circles, 3Mons post–MI = red circles **(G.)** Representative 3Mons post–MI PV loops ± CBSCs, the PV loops is shifted

Author Manuscript Author Manuscript Author Manuscript Author Manuscript

rightward in the VEH group. **(H.)** EDPVR is significantly shifted rightward in the VEH–treated animals vs. CBSC treatment while **(I.)** shows no significant change in ESPVR between groups 3Mons post–MI. **(J.)** Representative PV loops during dobutamine (DOB) challenge (2.5μg/kg/min.) 3Mons post–MI ± CBSCs. VEH + DOB = dashed red line/red squares, CBSC + DOB = dashed blue line/blue circles. **(K.)** No significant difference in the EDPVR between groups + DOB while **(L.)** demonstrates a significant difference in the ESPVR, indicating preserved contractile reserve in the CBSC group. N = 5 in each group.

Author Manuscript Author Manuscript Author Manuscript Author Manuscript

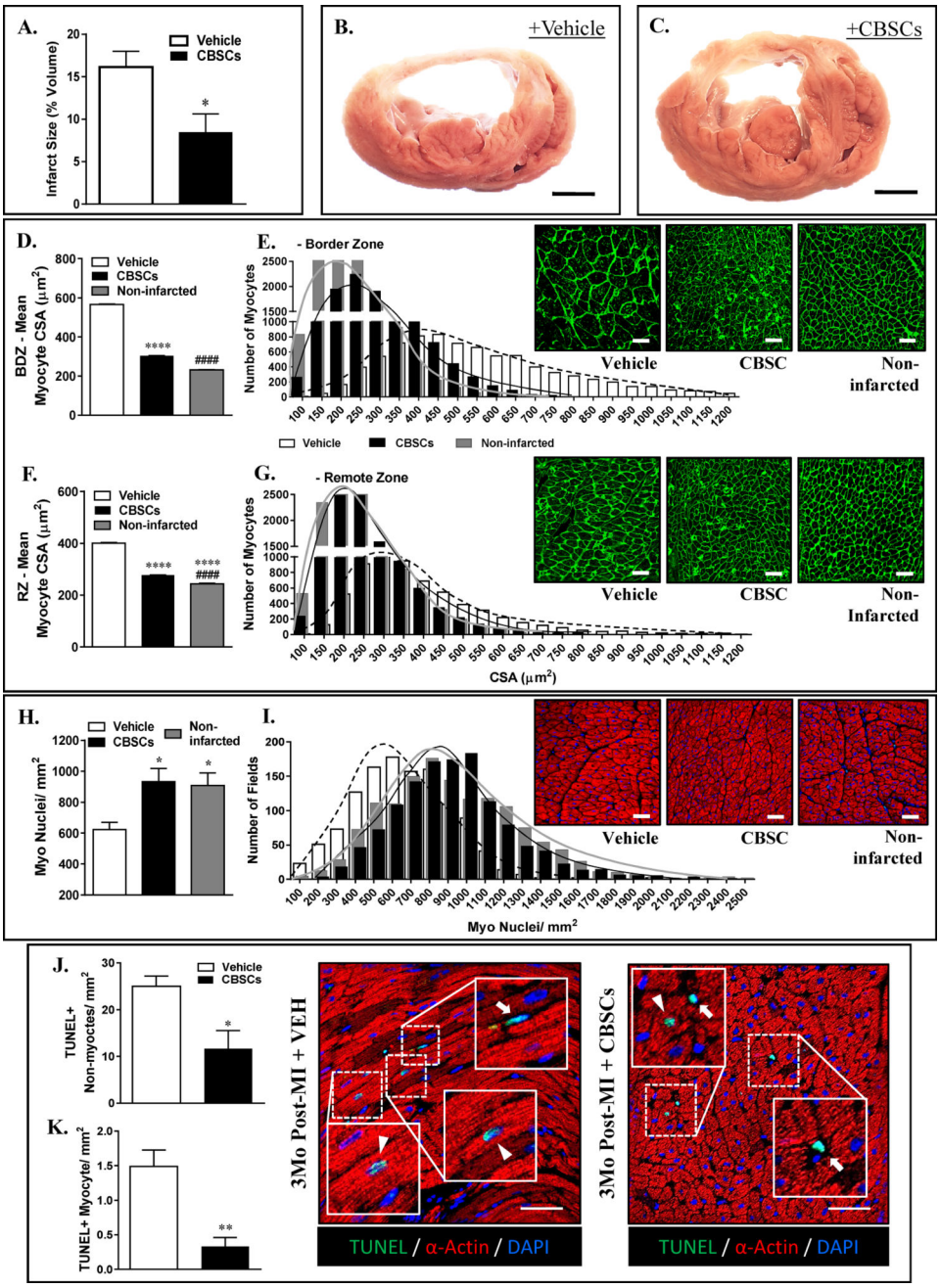

Figure 7. CBSCs Reduce Scar Size, Inhibit Pathological Hypertrophic Remodeling, Preserve Myocyte Nuclear Density & Reduce Cardiac Myocyte Death

Gross anatomy morphometric analysis for scar size, myocyte cross–sectional area (CSA), myocyte nuclear density and TUNEL staining was performed 3 Mons' post IR/MI or in non-infarcted controls. **(A.)** 2–fold reduction in scar size with CBSC treatment **(B. & C.)** Representative gross anatomy cross–sections of mid-myocardium ± CBSCs. Scale bar = 10mm. **(D.)** Average myocyte CSA in the border zone (BDZ) and **(E.)** myocyte CSA distribution within group and representative 40× confocal images of WGA staining. **(F.)** Average myocyte CSA in the remote zone (RZ) and **(G.)** myocyte CSA distribution within

Author Manuscript Author Manuscript Author Manuscript Author Manuscript

group and representative 40× confocal images of WGA staining. **(H.)** Average myocyte nuclei per mm^2 and **(I.)** distribution of nuclear density per group within viable tissue (BDZ and RZ combine). **(J.)** The mean number of $TUNEL^+$ non-myocytes per mm^2 and **(K.)** the mean number of $TUNEL^+$ myocytes per mm^2 of cardiac tissue is reduce in the CBSC group within viable tissue (BDZ and RZ combine). Representative confocal images of $TUNEL^+$ myocytes (arrowheads) and non-myocytes (arrows) in VEH– and CBSC–treated animals at 3Mon post-MI. Scale bar = 50μm. N = 5 in each group. p–value [*] ≤ 0.05, [**] ≤ 0.005, [****] ≤ 0.0001 vs. VEH–treated group, and [####] ≤ 0.0001 vs. CBSC group.

Author Manuscript Author Manuscript Author Manuscript Author Manuscript

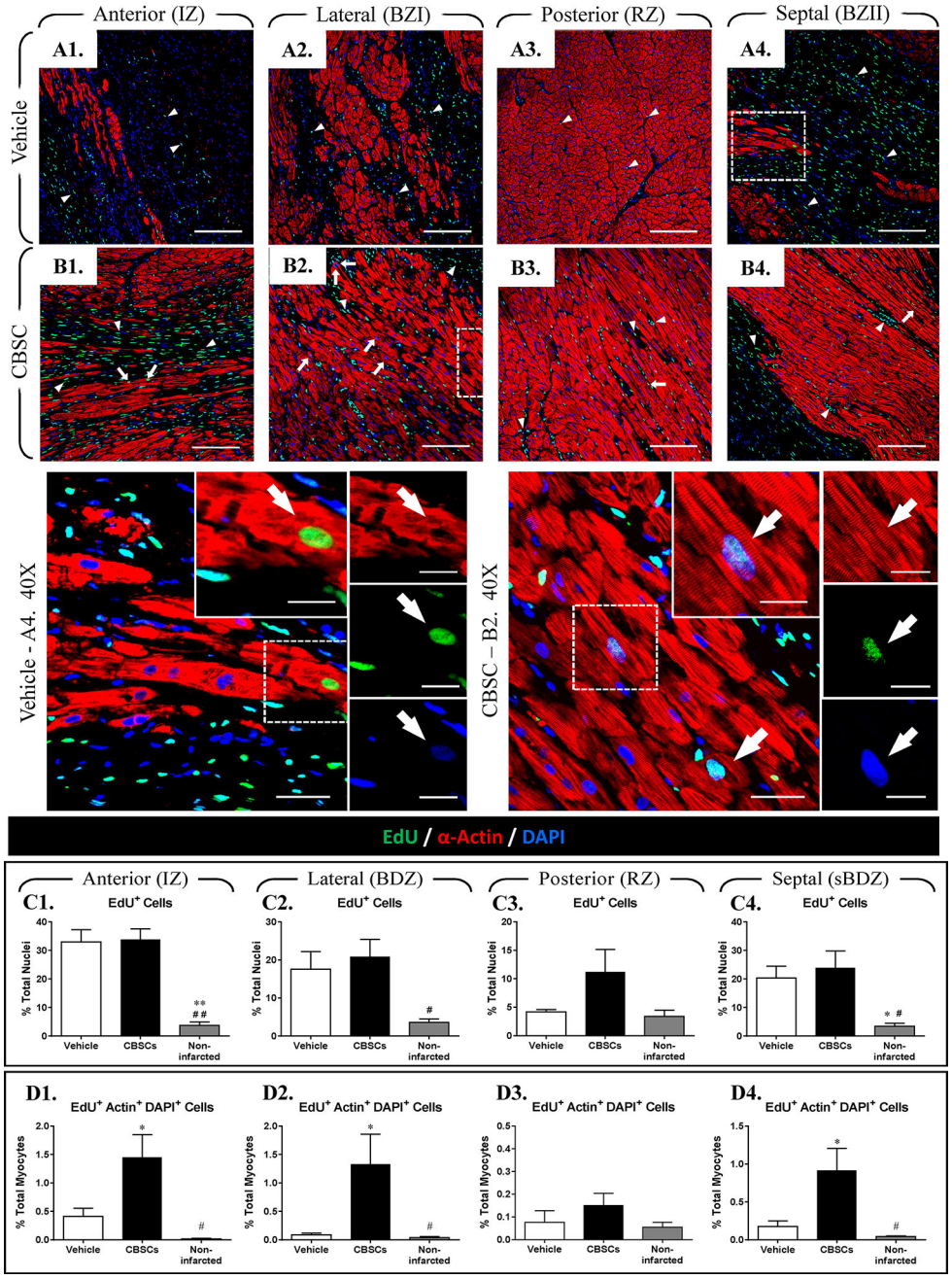

Figure 8. CBSC Treatment Increases EdU$^+$ Myocytes in the Border Zones

EdU$^+$ cells were imaged and quantified at 3Mons' post–MI in **(A)** VEH–, **(B)** CBSC–treated heart or non-infarcted controls **(A1. –A4.)** Representative confocal images (20×) from the four distinct regions of the myocardium post IR/MI + VEH. **(B1. –B4.)** Representative confocal images (20×) from the four distinct regions of the myocardium post IR/MI + CBSCs. 40× representative confocal images illustrates EdU$^+$ myocytes and non-myocytes from hearts ± CBSCs. EdU (green), α-Actin (red) and DAPI (blue). Arrows = myocytes, arrowheads = non–myocytes. 20× scale bars = 200μm, 40× scale bars = 50μm and zoom/ channel breakdown scale bars = 25μm. **(C1. – C4.)** Quantification of total EdU$^+$ cells as a

Author Manuscript Author Manuscript Author Manuscript Author Manuscript

percentage of total $DAPI^+$ in each region. **(D1. – D4.)** Quantification of total $EdU^+Actin^+DAPI^+$ cells as a percentage of total $Actin^+DAPI^+$ (myocyte) in each region. N = 5 in VEH- and CBSC- group. N = 3 in non-infarcted controls. p-value [*] ≤ 0.05, [**] ≤ 0.005 vs. VEH, [#] ≤ 0.05 [##] ≤ 0.005 vs. CBSC.